ATLAS
HEC Note-109
2 Mar 2001

Modeling of the HEC Electronics Chain

L.Kurchaninov

MAX-PLANCK-INSTITUT FÜR PHYSIK
Werner-Heisenberg-Institut
Föhringer Ring 6 80805 München

Abstract. In this Note the model for the HEC electronics chain is presented. The components of the chain are described by rational transfer functions in frequency domain. The signal waveforms in time domain are obtained by using the partial fractions expansion method. The noise is also described both in frequency and time domain.

1. INTRODUCTION

The detailed description of the electronics chain response is required for the HEC calibration and physics data analysis. The knowledge of transfer functions of the chain components is also needed to identify and locate possible malfunctioning parts. The scheme shown in Fig.1 represents the calibration and signal chain used in the HEC beam tests since June 1999. Almost the same chain is foreseen for the final ATLAS setup, so the test beam experience is useful to estimate the signal and noise characteristics for the future ATLAS conditions.

There are two possibilities to model the analog electronics, either to describe the transfer function analytically or numerically (PSPICE simulations). The PSPICE model is very powerful tool to study the details of the signal propagation through the chain. It is used to evaluate the influence of various imperfections, like cables termination condition, parasitic impedances, etc. The technological spread of nominal values can be simulated as well. But for the calibration procedure the PSPICE model can not be used since an analytical function to fit the signal shape is required.

The transfer function of the chain can be easily written in frequency domain following the schematics in Fig.1. All blocks can be described in terms of rational functions (combination of poles and zeros). The details of the modeling are given in section 3 for the calibration chain and in section 4 and 5 for the signal chain. The transformation to time domain is then done by using the partial fraction expansion method that is described in section 7.

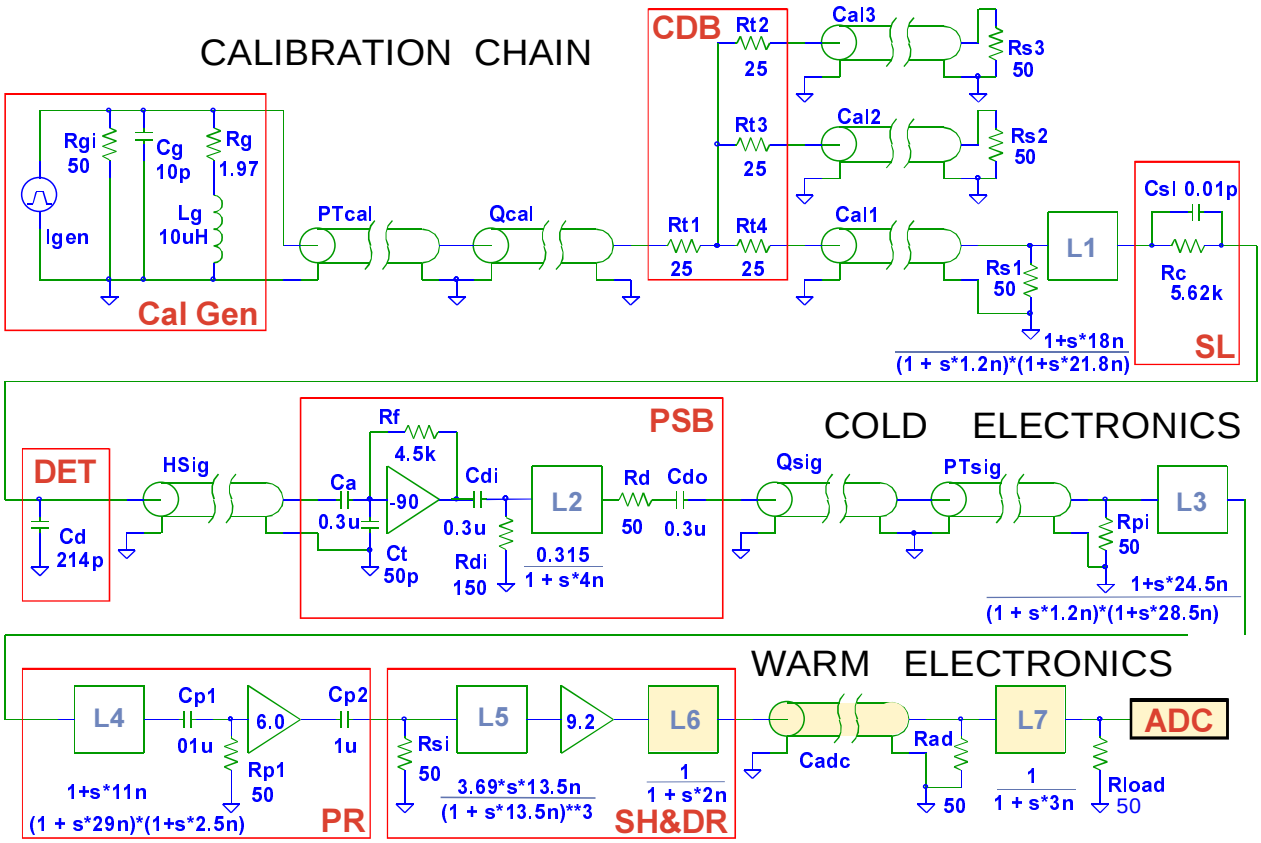

Figure 1: *Schematic diagram of the HEC electronics chain. All parameters are nominal at LAr temperature. The highlighted objects are specific for the test beam.*

The analytical approach has restricted possibilities and can not describe all the details of the chain. It is not very easy to include the reflections in cables. The parasitic impedances could in principal be described but the increasing of number of poles and zeros leads to dramatic rise of computing time and loss of precision. In the model presented below only “main” second-order effects are taken into account, like capacitance of strip line and 4 decoupling capacitors in the chain.

Electronics noise is very important aspect of the chain performance. The model presented in section 8 is based on the frequency domain approach. The calculations of the noise correlation function is performed by numerical calculation of Fourier integral.

2. DETECTOR CHARACTERISTICS

The detector characteristics determine both the signal waveform and noise values. One HEC ϕ-wedge has 88 readout cells, a part of them have identical geometry, hence the sets of model parameters are identical. The 51 of 88 readout cells have different parameters, they are numbered according to Fig.2. To make the numbering scheme useful also for physics simulation and analysis, the missing $\eta-\phi$ bins are also numbered.

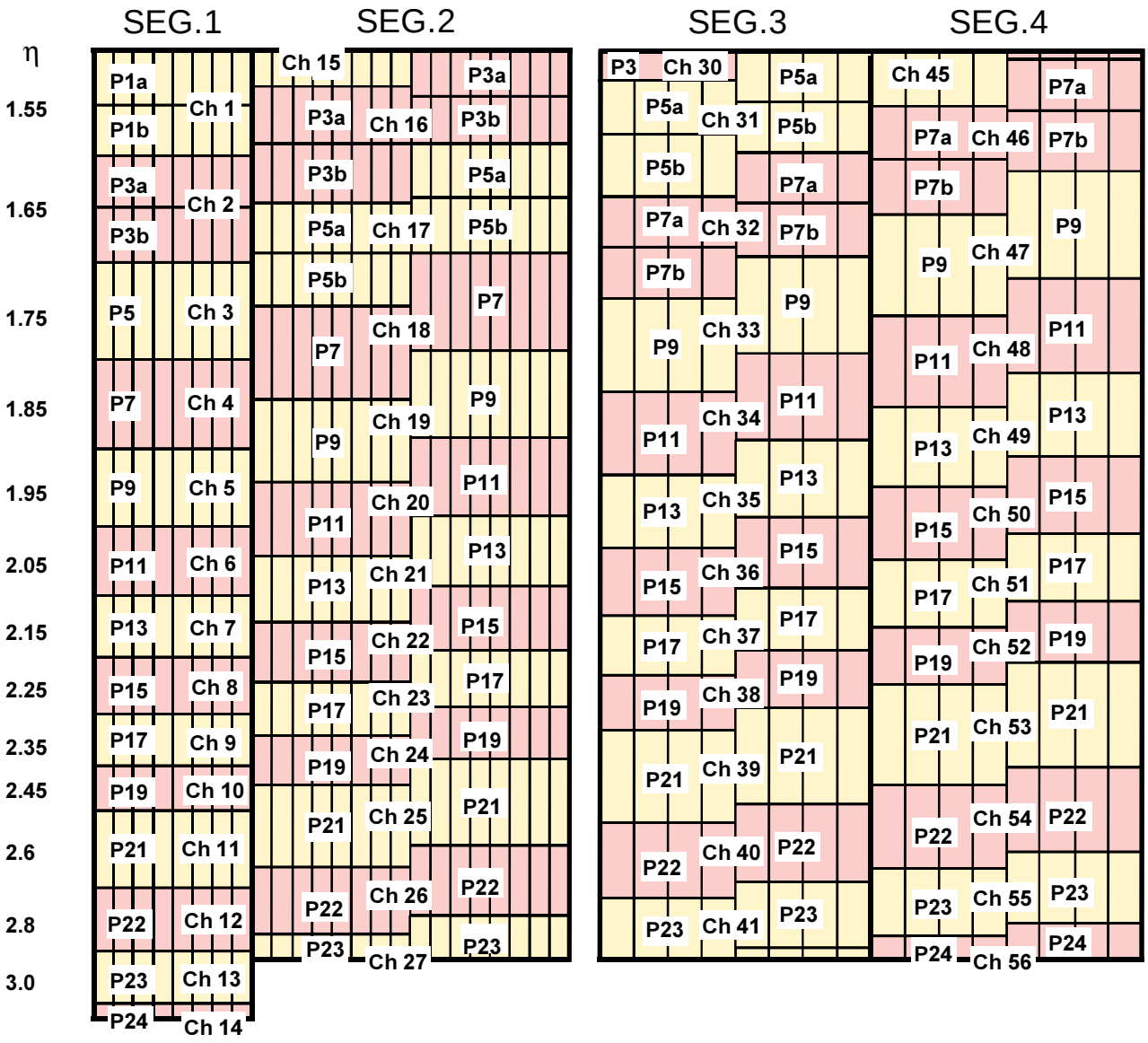

Figure 2: *Numbering of the HEC towers in each longitudinal segment (P1 .. P24) and numbering of readout channels in the wedge (Ch1 .. Ch56) .*

The most important characteristics of a detector is its capacitance, that determines the signal rise time and noise value. The HEC capacitance is a complicated function of frequency due to the high resistive layers in the gap. A rough estimation shows that capacitance is approaching to its high frequency asymptotic value (pure geometric capacitance of the gap) as $\sim f^{-1/2}$ with typical corner frequency of *~ 0.1 MHz*. So the effect in the working frequency range (*~10 MHz*) is about 1%. In the model this effect is neglected. The capacitance of double gap, connected to the preamplifier input has been calculated using simple equation for flat capacitance, neglecting the edge effects and presence of tie rods in some cells. The result of this calculations is presented in Tab.1.

Table 1: *Capacitance and cable length for HEC readout channels*

CHANNEL	LSEG	PAD	Cd, PF COLD	Cd, PF WARM	CABLE, M
1	1	1,2	215.49	141.77	0.39
2	1	3,4	213.76	140.63	0.53
3	1	5,6	339.54	223.38	0.76
4	1	7,8	270.95	178.26	0.79
5	1	9,10	217.03	142.78	0.99
6	1	11,12	174.36	114.71	1.02
7	1	13,14	140.40	92.37	1.17
8	1	15,16	113.26	74.51	1.20
9	1	17,18	91.48	60.19	1.31
10	1	19,20	73.96	48.66	1.35
11	1	21	223.35	146.94	1.57
12	1	22	147.31	96.91	1.60
13	1	23	97.20	63.95	1.76
14	1	24	23.52	15.47	1.79
15	2	1,2	151.25	99.51	0.32
16	2	3,4	220.30	144.93	0.69
17	2	5,6	202.76	133.39	0.79
18	2	7,8	323.70	212.96	0.78
19	2	9,10	259.37	170.64	1.00
20	2	11,12	208.44	137.13	1.00
21	2	13,14	167.91	110.47	1.19
22	2	15,16	135.51	89.15	1.26
23	2	17,18	109.51	72.05	1.46
24	2	19,20	88.58	58.28	1.53
25	2	21	267.00	175.66	1.75
26	2	22	176.23	115.94	1.80
27	2	23	69.77	45.90	1.93
28	2	24	0.00	0.00	0.00
29	3	1,2	0.00	0.00	0.00
30	3	3,4	112.00	73.68	0.42
31	3	5,6	224.00	147.37	0.50
32	3	7,8	202.00	132.89	0.65
33	3	9,10	323.50	212.83	0.76
34	3	11,12	260.50	171.38	0.78
35	3	13,14	209.50	137.83	1.01
36	3	15,16	169.50	111.51	1.03
37	3	17,18	137.00	90.13	1.23
38	3	19,20	112.00	73.68	1.23
39	3	21	335.50	220.72	1.44
40	3	22	220.00	144.74	1.47
41	3	23	156.00	102.63	1.66
42	3	24	0.00	0.00	0.00
43	4	1,2	0.00	0.00	0.00
44	4	3,4	0.00	0.00	0.00
45	4	5,6	217.00	142.76	0.40
46	4	7,8	242.00	159.21	0.50
47	4	9,10	383.50	252.30	0.75
48	4	11,12	308.00	202.63	0.77
49	4	13,14	248.50	163.49	1.00
50	4	15,16	201.00	132.24	1.02
51	4	17,18	162.50	106.91	1.20
52	4	19,20	131.50	86.51	1.22
53	4	21	395.00	259.87	1.43
54	4	22	261.00	171.71	1.45
55	4	23	173.00	113.82	1.63
56	4	24	64.00	42.11	1.67

The cables connecting gaps and preamplifiers have length between 0.3 and 1.9 m for different readout channels (see Tab.1). The signal distortion in these cables is negligible and not described in the model. But for the noise calculations these cables are taken into account since the influence to noise is more significant.

Detector is considered as an ideal current source. The original shape of the current is determined by the electrons drift in the liquid argon. In the case of uniform ionization and absence of electrons caption, this shape is triangular with initial ionization current *Io* and drift time τdr:

$$Ip(t) = Io \cdot \left(1 - \frac{t}{\tau dr}\right) \qquad \text{for} \quad 0 < t < \tau dr \tag{1}$$

The time of signal formation on the pad with dimension of 10-20 cm is in sub-*ns* region and not taken into account. The small inductance of lines connecting pads and cables are also not included in the model. The nominal value of drift time is *450 ns*, this value is typical for the beam tests and expected for the ATLAS conditions as well. The theoretical value of ionization current for energy deposited in LAr of *1 MeV* is *7.14 nA*. This value is in good agreement (within 2-3%) with the test beam data.

3. CALIBRATION CHAIN

The calibration current to preamplifier input is formed in calibration chain (the upper part of Fig.1). The exponential signal is produced by inductance *Lg* from rectangular pulse. The details of the generator circuit can be found in paper [1]. Since the real inductance has internal resistivity (Rg on Fig.1), the pulse shape is not pure exponential, there is a small (~7%) fraction of step. In frequency domain the signal can be easily derived as follows:

$$Ig \cdot Rl \cdot \frac{\alpha + s \cdot \tau c}{s \cdot (1 + s \cdot \tau c)}, \quad \text{where} \quad \alpha = \frac{Rg}{Rl + Rg}, \quad \text{and} \quad \tau c = \frac{Lg}{Rl + Rg} \tag{2}$$

Here *Rl* is the total loading impedance of generator, formed by the parallel connection of internal resistance *Rig* and external termination. The value of current *Ig* is controlled by DAC level. The nominal values of parameters are presented in Tab.2

Important consequence of eq.2 is that the calibration signal depends not only on the intrinsic generator parameters but on the loading impedance as well. So the shape is different for laboratory conditions (50 Ω termination), for the HEC chain at room temperature and for LAr temperature (cables have temperature dependent serial resistance, see below).

There are two parasitic effects which are not described in the model of calibration pulse (eq.2): injected charge and command feedthrough (see [1]). Fig.2 demonstrates the calibration signal for DAC level 2000 measured on the generator output with 50 Ω termination. The relative contribution of the parasitic effects becomes less with increasing the DAC value. Studies of the calibration waveforms show that this contribution is neglectable for the DAC level grater than ~10000.

The calibration pulse (eq.2) is distorted when propagates through calibration PigTail (line PTcal in Fig.1), Quadrant cable (line Qcal) and HEC calibration lines (Cal1, Cal2, Cal3). The Pig Tail is a coaxial 50Ω kapton cable of 2.7 m length both in test beam setup and in ATLAS. The Quadrant and HEC cables are also coaxial 50Ω Habia lines. The length of Qcal is 5.6m in the test beam setup, the longer cables of 6.5m are in production for ATLAS. The HEC calibration lines are

as long as 3.6m both in test beam setup and in ATLAS. So the total calibration cables length is 11.9m in beam tests and 12.8m is expected for the final ATLAS setup.

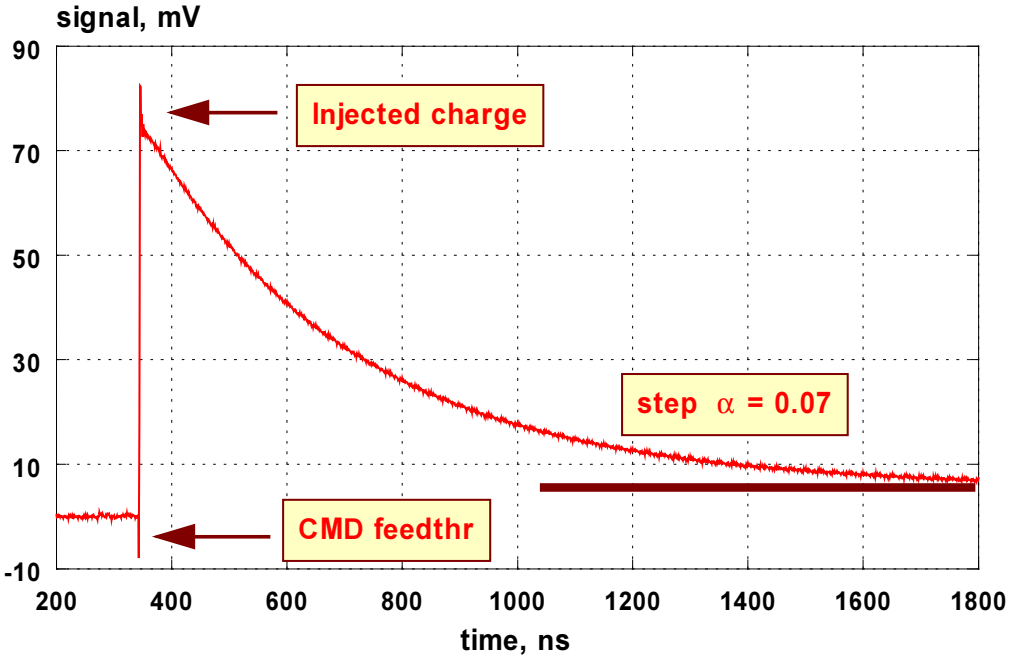

Figure 3: *Calibration pulse on the generator output.*

In the model all 3 parts of the calibration line are described by one transfer function The studies of the cable characteristics can be found in Note [2]. It has been shown that the impulse response is reasonably described by 1 zero and 2 poles:

$$\frac{ac\cdot(1+s\cdot\tau zc)}{(1+s\cdot\tau oc)\cdot(1+s\cdot\tau pc)},\quad \text{where attenuation}\quad ac=\frac{Rcc}{Rt+Rcc} \tag{3}$$

where *Rcc* is the serial resistance of central wire and *Rt* is the cable termination resistor (normally 50 Ω). This function is represented in Fig.1 by Laplace object L1.

It can be seen in Fig.4 that model (3) describes the signal distortion with precision ±1% (bigger deviation of a few points in the signal beginning is probably due to some imperfections of measurement. The precision of model can be improved by using a more complicated function. For instance, 2 zeros and 3 poles give twice less residual. But it was found that function (3) is precise enough in terms of description of final calibration waveform.

In the case of generator connected to terminated cable, the external loading impedance of generator *Rl* can be estimated as follows:

$$Rl=\frac{(Rt+Rcc)\cdot Rig}{Rt+Rcc+Rig} \tag{4}$$

All parameters in eq.3 depend on the cable length. The values placed in Tab.2 correspond to the nominal length of HEC calibration cables. The parameters have been found from the waveform oscilloscope measurements in laboratory conditions at room temperature and in LN_2. The room

temperature measurements have been also performed in different points of real test beam setup during the technical run in February 2000.

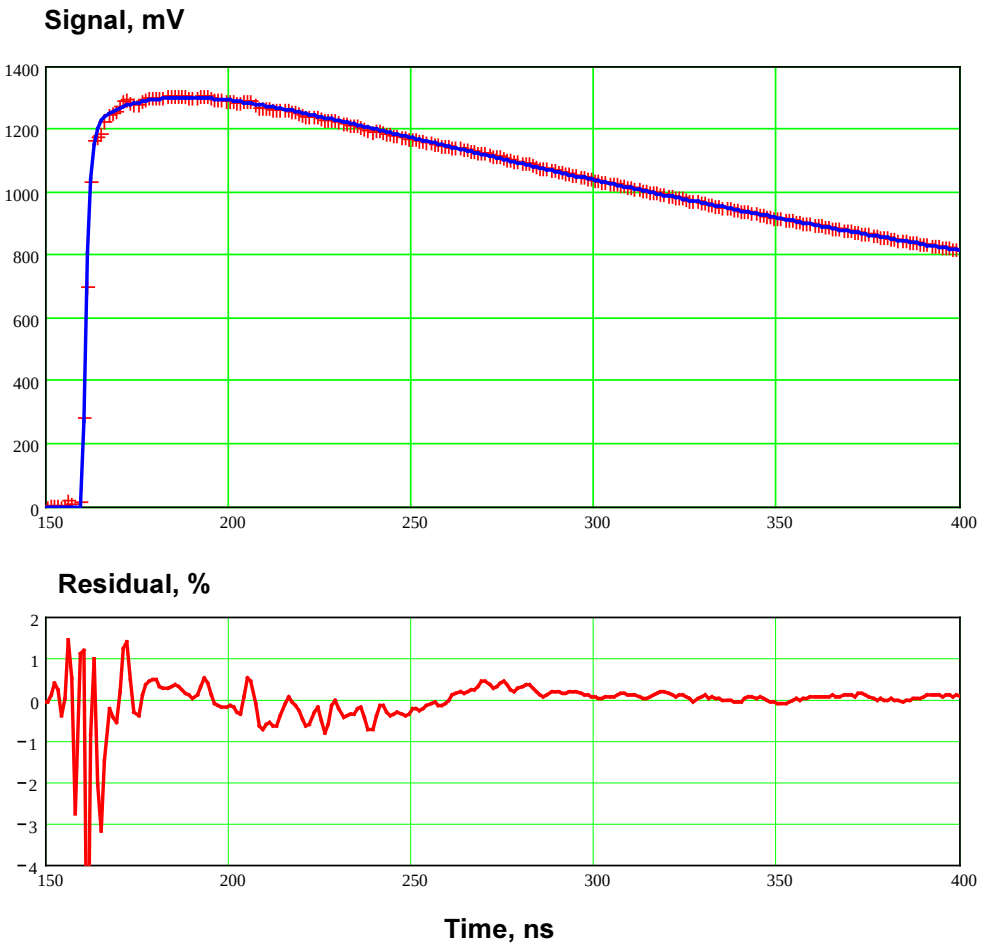

Figure 4: *Calibration pulse after 9m of Habia cable in LN_2. The response is modeled by eq.3.*

Another important component of the calibration chain is the calibration distribution board (block CDB on Fig.1). The passive splitting of signal guarantees the cables matching from both ends. Oscilloscope measurements show that there are now reflections in lines therefore the CDB can be described in the model simply as factor 1/3 without any shape deformation.

The calibration current to preamplifier input is formed by calibration resistors *Rc*, located on the HEC strip lines (SL). It is expected that a small parasitic capacitance *Csl* connected parallel to the resistor can appear due to the inter-electrode coupling on the SL. There were no dedicated measurements of the SL impedances done up to now. The value of *Csl* in Tab.2 has been obtained from the calibration waveforms analysis. Typically it is small enough to be neglected, nevertheless it is included into the model since one additional zero in transfer function does not complicate the transformation to time domain.

The transfer function of SL can be presented as:

$$(1 + s \cdot \tau sl) / Rc \qquad \text{where} \qquad \tau sl = Rc \cdot Csl \tag{5}$$

Multiplying functions (2), (3) and (5) one can get the final expression of the calibration current in frequency domain. The CDB attenuation factor 1/3 is also included

$$Ic(s) = Ig \cdot \frac{Rl \cdot ac}{3 \cdot Rc} \cdot \frac{(\alpha + s \cdot \tau c) \cdot (1 + s \cdot \tau zc) \cdot (1 + s \cdot \tau sl)}{s \cdot (1 + s \cdot \tau c) \cdot (1 + s \cdot \tau oc) \cdot (1 + s \cdot \tau pc)} \qquad (6)$$

All parameters are summarized in Tab.2 for room temperature and for LAr. The values for the ATLAS conditions are not exactly known yet. The calibration board used in the HEC beam tests is an intermediate version and some changes are foreseen for the final ATLAS system. The design is not completed yet so the model for the ATLAS signal is based on the test beam parameters. The longer calibration cables produce bigger distortions of signal. The cable parameters for the ATLAS chain are derived from the laboratory measurements done for different cable length. This recalculation is not very reliable since the measurements were done for Habia cables only, while the real setup is equipped by two types of cables connected in series.

Table 2: *Typical values of the calibration chain parameters.*

PARAMETER	TB WARM	TB COLD	ATLAS WARM	ATLAS COLD
Ig, μA/DAC	**1.48**	**---**	**---**	**---**
Lg, μH	**10.0**	**---**	**---**	**---**
Rg, Ω	**1.97**	**---**	**---**	**---**
Rig, Ω	**50**	**---**	**---**	**---**
Length, m	**11.9**	**---**	**12.8**	**---**
Delay, ns/m	**5.75**	**5.68**	**5.75**	**5.68**
Rt, Ω	**50**	**50**	**50**	**50**
Rcc, Ω	**14.1**	**5.4**	**15.2**	**5.8**
τzc, ns	**12.2**	**18.0**	**12.5**	**18.3**
τpc, ns	**18.6**	**21.8**	**19.3**	**22.5**
τoc, ns	**1.9**	**1.2**	**2.1**	**1.3**
Splitting	**1/3**	**1/3**	**1/3**	**1/3**
Rc, Ω	**5630**	**5620**	**5630**	**5620**
Csl, pF	**~0.1**	**~0.1**	**~0.1**	**~0.1**

It will be shown in section 7 that in the case of the HEC chain it is more convenient to deal with the derivative of calibration current *Ic'(t)*. In frequency domain this function is described by expression (6) where the multiplier *1/s* is removed. The expression in time domain can be easily obtained by symbolical inverse Laplace transform. For $t>0$ the signal is the sum of 3 exponential functions:

$$\frac{d}{dt} Ic(t) = Ig \cdot \frac{Rl \cdot ac}{3 \cdot Rc} \cdot \frac{\tau zc \cdot \tau sl}{\tau oc \cdot \tau pc} \cdot \left[\delta(t) + Fc \cdot \exp(-\frac{t}{\tau c}) + Fp \cdot \exp(-\frac{t}{\tau pc}) + Fo \cdot \exp(-\frac{t}{\tau oc}) \right] \qquad (7)$$

with coefficients:

$$Fc = \frac{\left(\frac{1}{\tau sl} - \frac{1}{\tau c}\right)\cdot\left(\frac{1}{\tau zc} - \frac{1}{\tau c}\right)\cdot\left(\frac{\alpha}{\tau c} - \frac{1}{\tau c}\right)}{\left(\frac{1}{\tau oc} - \frac{1}{\tau c}\right)\cdot\left(\frac{1}{\tau pc} - \frac{1}{\tau c}\right)}, \quad Fp = \frac{\left(\frac{1}{\tau sl} - \frac{1}{\tau pc}\right)\cdot\left(\frac{1}{\tau zc} - \frac{1}{\tau pc}\right)\cdot\left(\frac{\alpha}{\tau c} - \frac{1}{\tau pc}\right)}{\left(\frac{1}{\tau c} - \frac{1}{\tau pc}\right)\cdot\left(\frac{1}{\tau oc} - \frac{1}{\tau pc}\right)}, \quad Fo = \frac{\left(\frac{1}{\tau sl} - \frac{1}{\tau oc}\right)\cdot\left(\frac{1}{\tau zc} - \frac{1}{\tau oc}\right)\cdot\left(\frac{\alpha}{\tau c} - \frac{1}{\tau oc}\right)}{\left(\frac{1}{\tau c} - \frac{1}{\tau oc}\right)\cdot\left(\frac{1}{\tau pc} - \frac{1}{\tau oc}\right)} \quad (8)$$

The calibration signal can be calculated as integral of eq.7. An example of signal measured on the strip line level and prediction obtained from (7) is shown in Fig.5.

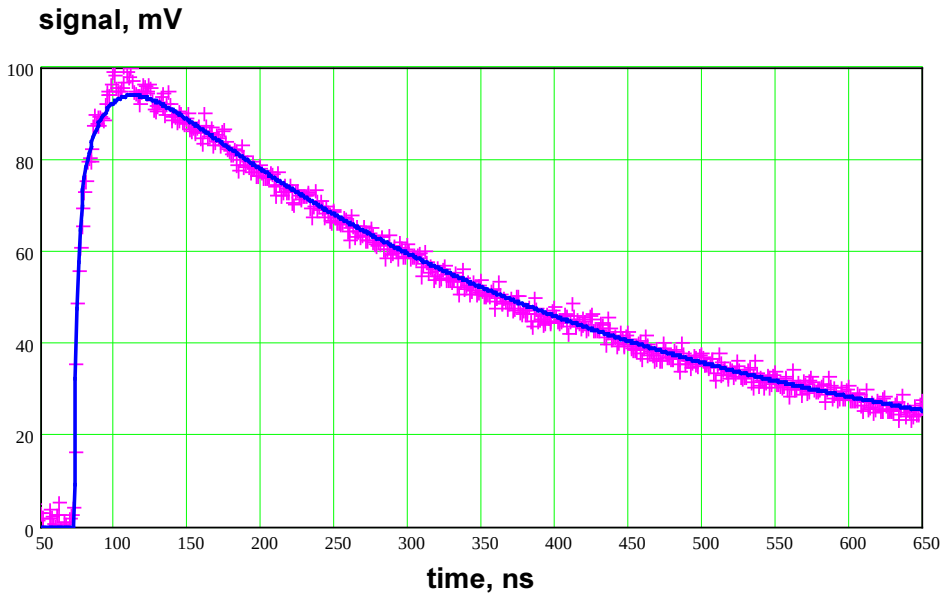

Figure 5: *Calibration pulse measured on the strip line level and it's model function.*

4. COLD ELECTRONICS

Current from the detector is amplified in preamplifying and summing boards (block PSB in Fig.1) . There are 3 components here relevant for the signal shaping – preamplifier, driver and decoupling capacitors. Then PSB output is connected to patch panels by Habia cables (line Qsig in Fig.1) of 5.6m length in test beam setup, in ATLAS it's length is expected to be 6m. From patch panel to the cryostat feedthrough the signals are transmitted through 2.7m Pig Tails (line PTsig in Fig.1). There are 2 decoupling capacitors affecting the signal shape – on the driver input and driver output. All these components are presented in the middle part of the scheme in Fig.1, they are referred to as Cold Electronics.

The preamplifier is designed to have input impedance $Rin = 50\ \Omega$ at LAr temperature for the purpose of cables matching. The first transistor is optimized for the noise performance, it consists of 100 gates, therefore it's capacitance *Ca* is not negligible. This capacitance is connected in parallel to the detector capacitance *Cd*, increasing the signal rise time. Another effect of Ca is the reflections in HEC cables, this effect is small and not taken into account. The second element of GaAs chip is the line driver. It has been found that this circuit introduces a small integration in few *ns* range. It is described by one pole with time constant τd (Laplace object L2 on Fig.1). The

GaAs chip transfer coefficient *Rp* is determined by the internal preamplifier feedback resistor and driver gain. So, the transfer function of PSB can be written as follows:

$$\frac{Rp}{(1+s\cdot\tau a)\cdot(1+s\cdot\tau d)} \qquad \text{with} \quad \tau a = Ra\cdot(Cd+Ca) \tag{9}$$

Nominal values of parameters are presented in Tab.3.

Two decoupling capacitors *Cdi* and *Cdo* introduce a simple differentiation of the signal. The last capacitor is connected in series with the preshaper input capacitor *Cp1*. The last one is present only in the preshaper version.0 used in the test beam setup and not foreseen in the next version (see the next section). The time constants are much higher then typical shaping time, so the effect of these capacitors is not very big. Nevertheless they are included into model since it makes the prediction of the final signal shape some ~1% better. The decoupling is described by the following function:

$$\frac{s\cdot\tau d1\cdot s\cdot\tau d2}{(1+s\cdot\tau d1)\cdot(1+s\cdot\tau d2)} \quad \text{with} \quad \tau d1 = 150\Omega\cdot Cdi \quad \text{and} \quad \tau d2 = 50\Omega\cdot\frac{Cdo\cdot Cp1}{Cdo+Cp1} \tag{10}$$

The distortions in cables are modeled following [2] by using 1 zero and 2 poles, like it is done for calibration line:

$$\frac{as\cdot(1+s\cdot\tau zs)}{(1+s\cdot\tau os)\cdot(1+s\cdot\tau ps)} \tag{11}$$

This function is represented in Fig.1 by Laplace object L3.

Multiplying (9), (10) and (11) one obtains the cold electronics transfer function:

$$Hc(s) = \frac{Rp\cdot as\cdot s\cdot\tau d1\cdot s\cdot\tau d2\cdot(1+s\cdot\tau zs)}{(1+s\cdot\tau a)\cdot(1+s\cdot\tau d)\cdot(1+s\cdot\tau d1)\cdot(1+s\cdot\tau d2)\cdot(1+s\cdot\tau os)\cdot(1+s\cdot\tau ps)} \tag{12}$$

Table 3: *Typical values of the cold electronics chain parameters*

PARAMETER	TB WARM	TB COLD	ATLAS WARM	ATLAS COLD
Ra, Ω	**65**	**50**	**65**	**50**
Rp, Ω	**700**	**750**	**700**	**750**
Ca, pF	**40**	**50**	**40**	**50**
τd, ns	**7**	**4**	**7**	**4**
Cdi, μF	**1**	**0.3**	**1**	**0.3**
Cdo, μF	**1**	**0.3**	**1**	**0.3**
Cp1, μF	**1**	**1**	**∞**	**∞**
Length, m	**8.3**	**---**	**8.7**	**---**
Delay, ns/m	**5.75**	**5.68**	**5.75**	**5.68**
as	**0.884**	**0.965**	**0.879**	**0.963**
τzs, ns	**13.3**	**24.5**	**13.6**	**24.7**
τps, ns	**17.2**	**28.5**	**17.7**	**28.9**
τos, ns	**1.6**	**1.2**	**1.7**	**1.3**

Parameters of the chain placed in Tab.3 are nominal, either design values or averaged over measured samples. The preamplifiers have technological spread of about ±10% so that the observed waveform can differ significantly from the nominal one. The PSBs currently used in the test beam setup are the first samples of the series production for ATLAS, so the set of parameters in ATLAS is identical to that of the test beam. The signal cable parameters are recalculated for ATLAS conditions on the basis of laboratory measurements. As it was mentioned in Section 3, this prediction is not very reliable, so the set of parameters will be corrected as soon as ATLAS data will be taken and analyzed.

5. WARM ELECTRONICS

The final signal shape is formed in the warm electronics (lowest part of Fig.1). There are 2 important components on the front end board (FEB) – preshaper and shaper. In the test beam setup the signal is transmitted to digitizing system through FEB driver and 3m twisted pair cables. These last parts are only beam tests specific and will be not present in the final ATLAS chain (highlighted objects in Fig.1). The nominal parameters of warm electronics components are shown in Tab.4.

The goal of preshaper (block PR in Fig.1) is to compensate the preamplifier rise time and make an additional integration in order to reach the final peaking time of 50 *ns*. This function is represented by Laplace object L4 in the schematics. Additional gain is introduced to adapt the shaper linearity range. There is a decoupling capacitor on the preshaper output that introduces the differentiation with time constant $\tau d3$:

$$\tau d3 = 50\Omega \cdot Cp2 \tag{13}$$

The preshaper transfer function is as follows:

$$\frac{Gp \cdot (1 + s \cdot \tau pz) \cdot s \cdot \tau d3}{(1 + s \cdot \tau i) \cdot (1 + s \cdot \tau o) \cdot (1 + s \cdot \tau d3)} \tag{14}$$

Details of the preshaper circuit can be found in the Review [3]. The test beam setup is equipped by the pre-production version.0 of the preshaper hybrids. The design parameters of this version differ from those implemented in the next generation (version.1) supposed to be produced for ATLAS. For instance, the zero time constant τpz has been adjusted for each HEC channel according to the following equations:

$$\tau pz = 47\Omega \cdot Cd \quad \text{in TB} \qquad \text{and} \qquad \tau pz = 50\Omega \cdot (Cd + Ca) \quad \text{for ATLAS} \tag{15}$$

Another difference in version.1 is that the signal distortion in cold cables have been taken into account so that the integration time constant τi and gain were changed significantly. The preshaper gain *Gp* for the rear HEC modules is twice high than for the front ones. This is done to compensate the difference of the calorimeter sampling ratios.

Fig.6 shows an example of the preshaper step response measured with stand alone hybrid in the laboratory conditions. Measurement was done with preshaper adjusted for the readout channel 1 (detector capacitance according to Tab.1). The precision of the model (14) is rather good excluding a region in the pulse origin, where the measured points have some irregularities.

The RC^2-CR shaper (object L5 in Fig.1) is common for all ATLAS liquid argon detectors. It's time constant τs has bean chosen from global optimization of the signal to noise ratio of the calorimeters. Different versions of the circuit are described in paper [4]. In the model the shaper is considered as an ideal one with the following transfer function:

$$3.69 \cdot Gs \cdot \frac{s \cdot \tau s}{(1 + s \cdot \tau s)^3} \qquad (16)$$

The shaper gain Gs is defined for the step response, that is why the multiplier of 3.69 appears in the frequency domain. In the test beam setup the only medium gain is used while in ATLAS all 3 gains will be processed. Several measurements of the signal waveforms in laboratory conditions and in the test beam setup demonstrate that the real circuits are described very well by the idealized function (16).

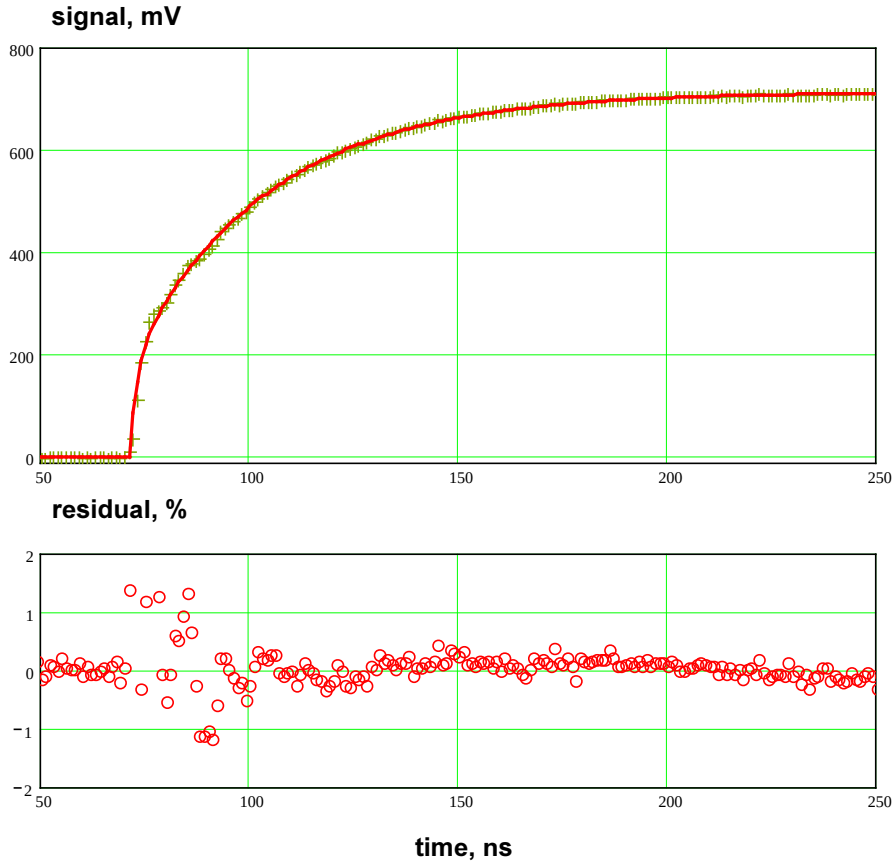

Figure 6: *Example of the preshaper step response and model function (13).*

In the HEC beam tests the early prototype of the FEB (version –1) is used. This board contains only analog part of the front-end electronics, the digitization is performed by a home-made ADC modules. So there are two components of the chain, specific for the HEC test beam setup – line driver installed on the FEB and cable connected to ADC modules. It has been found that these parts introduce short integration and can be modeled by 1 pole each.

In the ATLAS chain model one of these poles is present aiming to describe a possible signal integration in the analog pipeline circuit or in somewhere else. Since the value of this time

constant is not known for ATLAS conditions, it is fixed to 1 ns without any particular consideration. The function describing the last part of the chain is:

$$\frac{1}{(1+s\cdot\tau fd)\cdot(1+s\cdot\tau ac)} \tag{17}$$

The transfer function of the warm electronics is the product of functions (14), (16) and (17), resulting to:

$$Hw(s)=\frac{3.69\cdot Gs\cdot Gp\cdot(1+s\cdot\tau pz)\cdot s^2\cdot\tau s\cdot\tau d3}{(1+s\cdot\tau i)\cdot(1+s\cdot\tau o)\cdot(1+s\cdot\tau s)^3\cdot(1+s\cdot\tau fd)\cdot(1+s\cdot\tau ac)\cdot(1+s\cdot\tau d3)} \tag{18}$$

Parameters involved in this function for the test beam setup and expected values for ATLAS are collected in Tab.4.

Table 4: *Nominal values of the warm electronics chain parameters*

PARAMETER	TB	ATLAS
Gp front	**6.5**	**5.5**
Gp rear	**12.2**	**11.0**
τi, ns	**33.0**	**14.0**
τo, ns	**2.5**	**1.0**
Cp2, μF	**1**	**1**
Gs	**9.2**	**10.0**
τs, ns	**13.5**	**15.0**
τfd, ns	**2.0**	**1.0**
τac, ns	**3.0**	**0**

6. SIGNAL WAVEFORM

Equations (12) and (18) determine the complete chain transfer function. It consists of 2 zeros, 10 poles and 4-times differentiation. As can be seen from eq.6, the calibration pulse has multiplier *1/s*. When calibration response is calculated in frequency domain, this multiplier is cancelled with one of the multiplier *s* in the chain transfer function. The resulting expression can be interpreted as product of *derivative* of calibration pulse with the *step response* of the chain. So, the calculation in time domain is a convolution of function (7) with the chain step response calculated in time domain.

The ionization signal can be calculated in the same way by convoluting the derivative of ionization current with the chain step response. The first one can be easily obtained from expression (1):

$$\frac{d}{dt} Ip(t) = Io \cdot \left(\delta(t) - \frac{1}{\tau dr} \right) \qquad \text{for} \quad 0 < t < \tau dr \tag{19}$$

and the chain step response by definition is:

$$G(s) = \frac{Hc(s) \cdot Hw(s)}{s} \tag{20}$$

The last function (20) is too complicated to be transformed analytically to time domain. The only way to obtain it's expression is the partial fractions expansion method, well known in operational analysis. The idea is that any rational function (when number of poles is grater than the number of zeros) can be presented as a sum of poles:

$$\frac{(s + sz_1) \cdot (s + sz_2) \cdot \ldots \cdot (s + sz_m)}{(s + sp_1) \cdot (s + sp_2) \cdot \ldots \cdot (s + sp_n)} \equiv \sum_{k=1}^{n} \frac{D_k}{s + sp_k} \tag{21}$$

The coefficients D_k are determined by constants *sz* and *sp*. They can be found in 2 steps: first, the right-side sum is transformed to the common denominator. Then, the numerators of both left-side and right-side functions are expressed as a power series of *s*. Since these two numerators have to be identical, the polynomial coefficients are equal. This condition gives system of *n* linear equations for *n* coefficients D_k . The system can be solved numerically.

As soon as coefficients are found, then the transform to time domain is very simple since the inverse Laplace transform of a pole is exponential function:

$$\frac{1}{s + sp} \rightarrow \exp(-sp \cdot t) \qquad \text{for} \quad t > 0 \tag{22}$$

so that the chain step response can be expressed as:

$$G(t) = \sum_{k=1}^{14} D_k \cdot \exp(-\frac{t}{\tau p_k}) \tag{23}$$

where τp_k are 14 time constants appearing in the denominator of *G(s).* In the practice of the HEC signals reconstruction and analysis this method of the chain description is referred to as exponential expansion (EE) method since the step response is represented as a sum of exponents.

Equation (21) is true only when all poles have different time constants, that is formally not true for the HEC chain due to the triple pole of the shaper. In practice this problem is solved by substituting the triple pole by 3 poles with slightly different time constants. This approach is useful since it gives a possibility to model the real shaper circuit where 3 time constants can be not identical. The similar problem appears when function (23) is used to fit measured waveform. When during the fit iterations one of time constant approaches to another one, the method gives an unpredictable result. A special care has to be taken to avoid this situation.

When the step response (23) is known, the expression for the calibration signal can be obtained directly in time domain by convoluting functions (7) and (23). The convolution of two exponents with not equal time constants is:

$$\exp\left(-\frac{t}{\tau 1} \right) \otimes \exp\left(-\frac{t}{\tau 2} \right) = \frac{\tau 1 \cdot \tau 2}{\tau 1 - \tau 2} \left[\exp\left(-\frac{t}{\tau 1} \right) - \exp\left(-\frac{t}{\tau 2} \right) \right] \tag{24}$$

So the calibration signal is expressed as:

$$Uc(t) = Qc \cdot \left[G(t) + \sum_{i=1}^{3} \sum_{k=1}^{14} F_i \cdot D_k \cdot \frac{\tau c_i \cdot \tau p_k}{\tau c_i - \tau p_k} \left(\exp\left(-\frac{t}{\tau c_i} \right) - \exp\left(-\frac{t}{\tau p_k} \right) \right) \right] \qquad (25)$$

here Qc denotes the common multiplier in expression (7), F_i are 3 coefficients from (8) and τc_i are corresponding time constants of the calibration chain.

Function (25) potentially describes the real calibration signal with very high accuracy in the full time range. The experience shows that the precision of ±1% can be reached when only 2 time constants of the chain are free fit parameters. Normally the preshaper integration τi and shaper time constant τs are chosen for adjustment. For some problematic channels, the preamplifier rise time τa and strip line capacitance Csl has to be adjusted in addition. Fig.7 shows the calibration waveform for one of such problematic channels measured in August 2000 beam run and fit by function (25). The measurements done for DAC level of 2000, where the generator parasitic effects are still not very small.

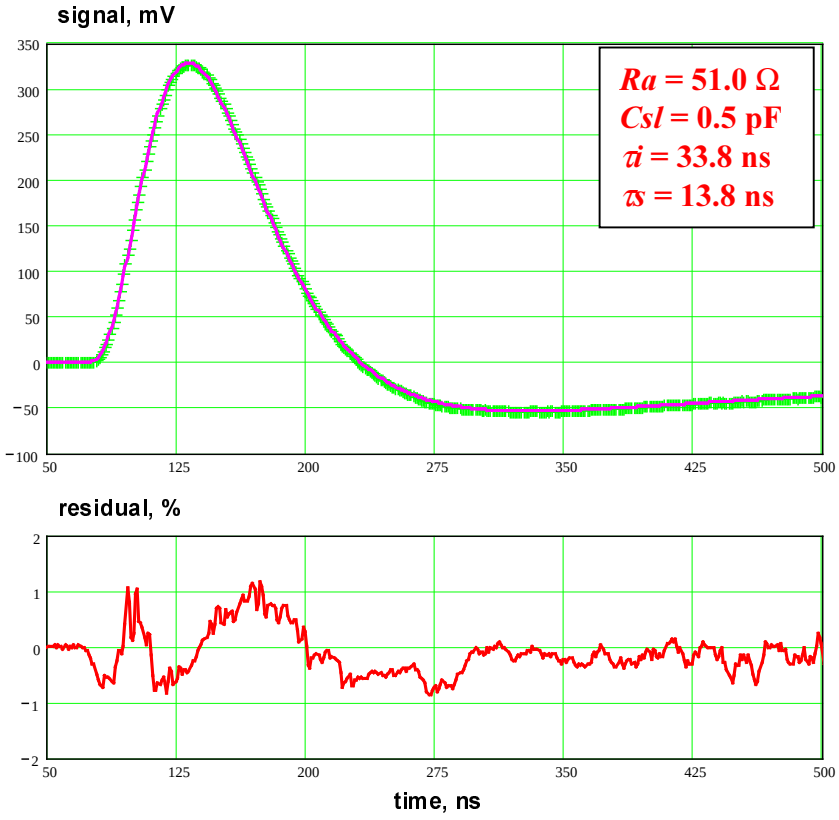

Figure 7: *Example of the calibration signal and model function (25) with adjusted parameters. Compare to nominal values in Tab.2, Tab.3 and Tab.4.*

There are two modes of calibration used in the beam tests, pulsing either all generators simultaneously or the single one. In the last case the waveform differs from the theoretical one due to crosstalk leakage of current to neighboring pads. Formally this waveform is not described by the model but the function (25) still can be used to fit data. The only difference is that the values of

adjusted parameters now do not correspond to the real values of the chain components. The typical precision of ±1% is also achievable in this case.

The ionization signal is the convolution of (19) and response (23). The convolution of (19) with one exponential function is done analytically giving the following expression:

$$Sp(t,\tau) \equiv \left(\delta(t) - \frac{1}{\tau dr}\right) \oplus \exp\left(-\frac{t}{\tau}\right) = \begin{cases} \left(1 + \frac{\tau}{\tau dr}\right) \cdot \exp\left(-\frac{t}{\tau}\right) - \frac{\tau}{\tau dr} & \text{for } t < \tau dr \\ \left(1 + \frac{\tau}{\tau dr} - \frac{\tau}{\tau dr} \cdot \exp\left(\frac{\tau dr}{\tau}\right)\right) \cdot \exp\left(-\frac{t}{\tau}\right) & \text{for } t > \tau dr \end{cases} \tag{26}$$

So, the ionization signal is the sum of 14 functions (26):

$$Up(t) = Ip \cdot \sum_{k=1}^{14} D_k \cdot Sp(t, \tau p_k) \tag{27}$$

Model of the ionization waveform (27) reproduce the real signals with typical accuracy of ± 1% in the full time window. Fig.8 demonstrates the signal from the first longitudinal segment produced by electrons 148 GeV measured in August 2000 run period. Chain parameters are fixed by using calibration waveform in this readout cell. The initial ionization current *Io* and electrons drift time τdr are fit parameters.

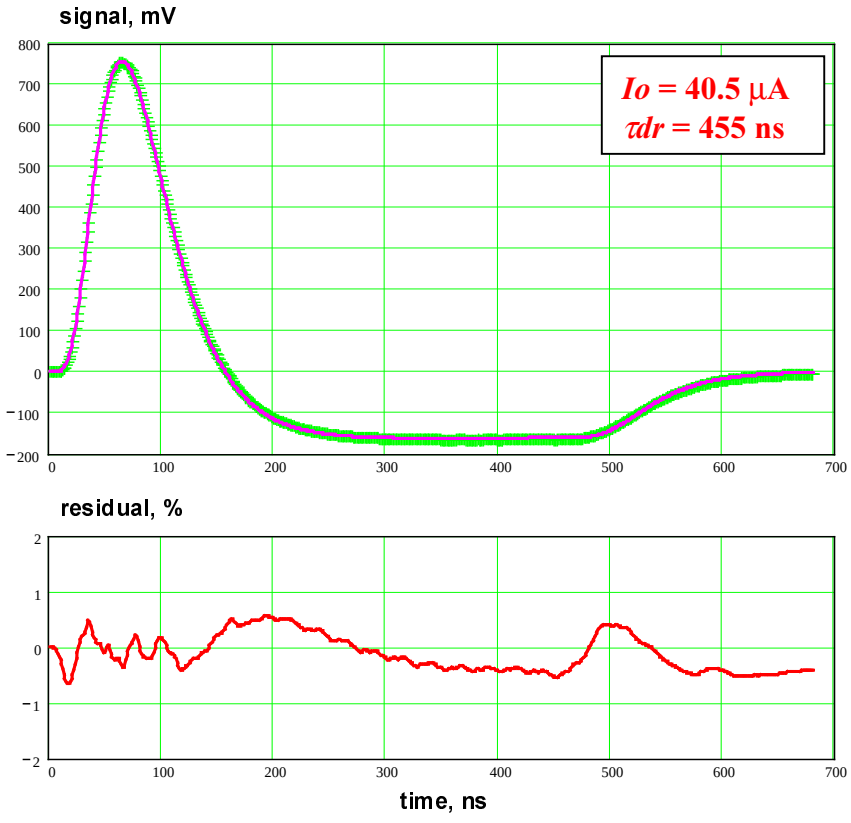

Figure 8: *Example of the ionization signal and model function (27) with fixed chain parameters.*

As can be seen from Tab.2 – Tab.4, there are many parameters different for present test beam setup and future ATLAS chain. It is expected that both calibration and ionization signals in ATLAS will be shorter (peaking time ~50 ns) and gain is higher. Fig.9 shows waveforms calculated for these two sets of parameters for readout channel 3 (*Cd* = 339 pF). For ionization current *Io* = 10 μA (visible energy of 1.40 GeV and total energy 32.8 GeV), the signal amplitude is 291 mV that gives the transfer coefficient of 29.1 KΩ or 8,9 mV/GeV. The calibration current is also 10 μA that is achieved with DAC = 4803 for the test beam setup and 4820 for the case of ATLAS.

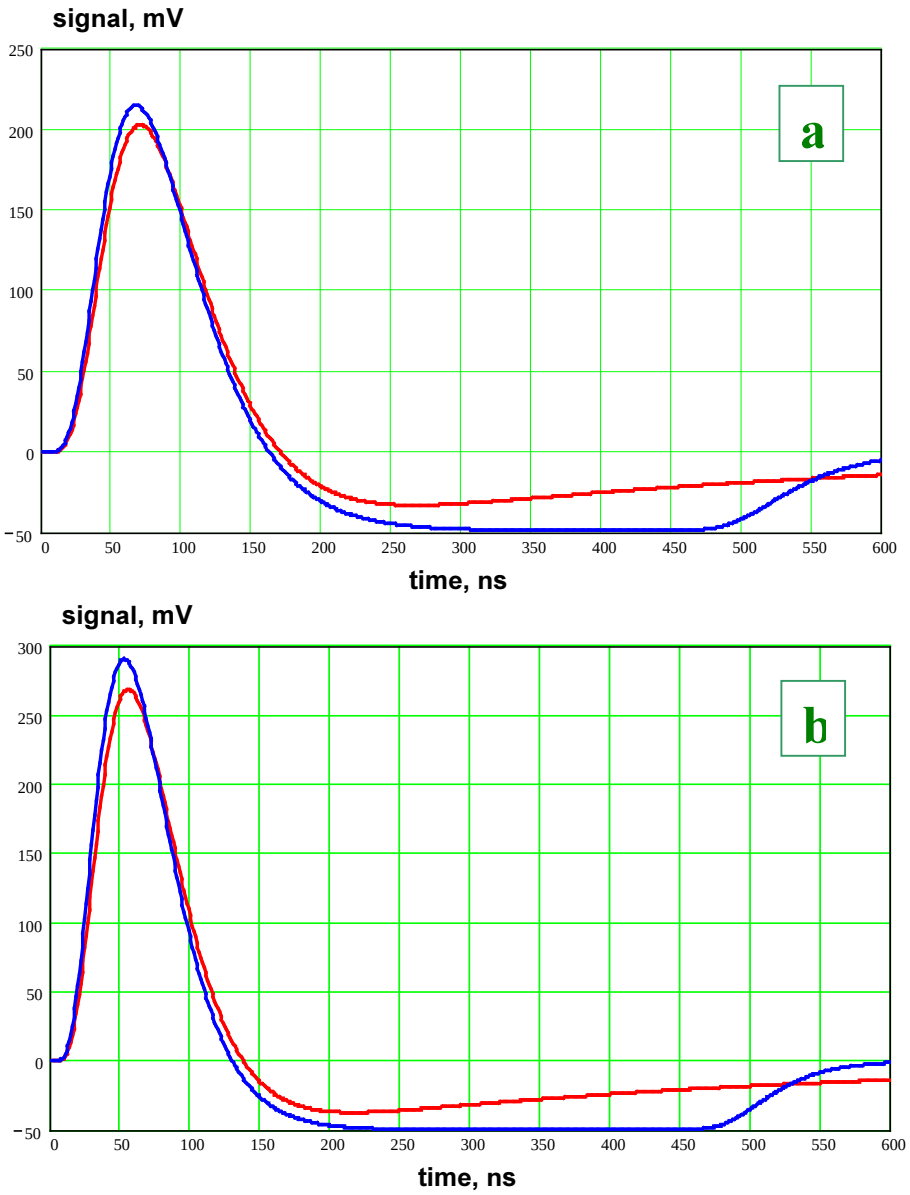

***Figure 9**: Nominal ionization (blue) and calibration (red) signals for test beam (a) and ATLAS (b) setup calculated for input current of 10 μA*

***Table 5**: Samples of ionization signal*

Sample number	Value
1	0
2	0.46555
3	1
4	0.69249
5	0.26841
6	0.01592
7	-0.09842
8	-0.14410
9	-0.16133
10	-0.16763
11	-0.16984
12	-0.17051
13	-0.17058
14	-0.17041
15	-0.17015
16	-0.16986
17	-0.16955
18	-0.16923
19	-0.16891
20	-0.16103
21	-0.11375
22	-0.05969
23	-0.02623
24	-0.01049
25	-0.00401
26	-0.00150
27	-0.00054
28	-0.00017
29	-0.00003
30	0

7. ELECTRONICS NOISE

Electronics noise can be calculated on the basis of simple model shown in Fig.10 with 2 independent noise sources on the preamplifier input - serial (or voltage) noise and parallel (or current) noise. This approach is widely used for the electronic noise description. Physically serial noise e_S represents the thermal noise of the first transistor and possible contribution of the second stage. Parallel source i_P describes the feedback resistor thermal noise and shot noise of all leakage currents. The amplifier in the diagram is noiseless with transfer coefficient *Rp* and input impedance *Ra*. The chain is presented by transfer function H(s) that is the product of functions (12) and (18) without multiplier *Rp*.

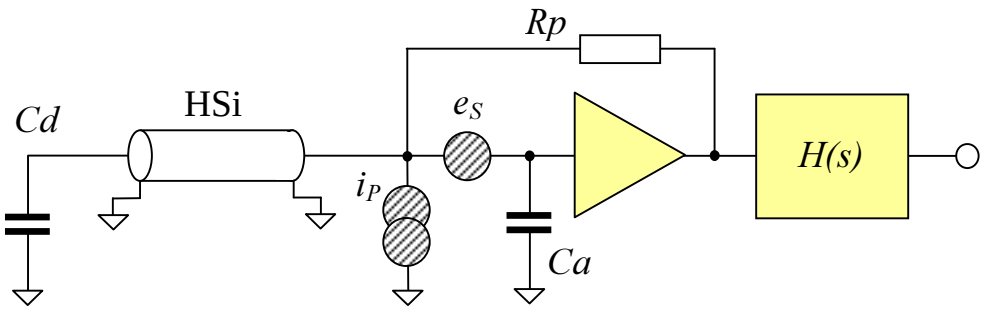

Figure 10: *Noise sources in the signal chain*

Usually the fluctuations e_S and i_P are characterized by spectral densities that are parameterized by equivalent noise resistances *Rnp* and *Rns* as follows:

$$\frac{d}{df}\overline{i_P^{\,2}} = \frac{4kT}{Rnp}\left(1+\frac{\omega s}{\omega}\right) \qquad \text{and} \qquad \frac{d}{df}\overline{e_S^{\,2}} = 4kT \cdot Rns \qquad (28)$$

Values of *Rnp* and *Rns* are found from measured noise spectrum. It has been observed that the parallel source of GaAs preamplifier has the flicker noise contribution with corner frequency ωs varying significantly from chip to chip. Values of noise parameters were extracted from laboratory measurements in liquid nitrogen. Afterwards it was found that in the test beam setup the noise values (except of few oscillating channels) are 10 – 20% bigger than in the laboratory conditions. Tab.6 shows 3 noise parameters for the noise model of pure GaAs chip and for the real setup. In further calculations the last set of parameters will be used.

Table 6: *Nominal values of the noise parameters*

Parameter	Preamplifier in LN	Full chain In LAr
Rns, Ω	**35**	**45**
Rnp, Ω	**700**	**400**
ωs, Mrad/s	**1.5**	**0.9**

Transmission line in Fig.10 represents the short HEC signal cables. This cable produces reflections that change the shape of spectral density and, as a consequence, the shape of noise autocorrelation function. In the model the cable is described by the well known equation of ideal transmission line (wave impedance ρ and propagation tine Tc) loaded by capacitor Cd:

$$Zc(\omega) = \rho \cdot \frac{1+\kappa(\omega)\cdot\exp(-2i\omega Tc)}{1-\kappa(\omega)\cdot\exp(-2i\omega Tc)} \quad \text{with reflection factor} \quad \kappa(\omega) = \frac{1-i\omega\rho Cd}{1+i\omega\rho Cd} \tag{29}$$

The total noise current to the preamplifier input i_N can be calculated using Ohm's law and taking into account that e_S and i_P are independent. Using parameterization (29) one can obtain:

$$\frac{d}{df}\overline{i_N{}^2} = \left|\frac{1+i\omega(Ca+Cd)Ra}{1+i\omega(Ca+Cc(\omega))Ra}\right|^2 \cdot \left(\frac{4kT}{Rnp}\left(1+\frac{\omega_S}{\omega}\right) + 4kT\cdot Rns\cdot\omega^2\left|Ca+Cc(\omega)\right|^2\right) \tag{30}$$

Where $Cc(\omega)$ is equivalent cable capacitance:

$$Cc(\omega) = 1/i\omega Zc(\omega) \tag{31}$$

The noise on the chain output Ue has spectral density calculated with transfer function as follows:

$$Se(\omega) \equiv \frac{d}{df}\overline{Ue^2} = \frac{d}{df}\overline{i_N{}^2}\cdot\left|Hc(i\omega)\cdot Hw(i\omega)\right|^2 \tag{32}$$

The electronics noise RMS value can be now calculated as

$$\sigma e = \left(\frac{1}{2\pi}\int_0^\infty Sn(\omega)d\omega\right)^{1/2} \tag{33}$$

It can be expressed in terms of input ionization current by dividing σe by the chain transfer coefficient (the output amplitude for Io=1). The resulting value is referred to as equivalent noise current (ENI) and frequently used as the integral noise characteristic of the chain. Another important value needed for optimization the digital signal processing is the noise autocorrelation function. It is defined as follows:

$$Ke(t) = \frac{1}{2\pi\cdot\sigma e^2}\int_0^\infty Se(t)\cdot\cos(\omega\cdot t)d\omega\ , \qquad Ke(0) = 1 \tag{34}$$

Integration in (33) and (34) is performed numerically. Fig.11(a) shows ENI measured in test beam August 2000 compared to calculations with equation (33). Noise correlation function (34) calculated for readout channel 2 is shown in Fig.11(b) in comparison with 4 corresponding readout cells of 2 HEC modules. The agreement is quite reasonable. Calculations show that the ENI expected for the ATLAS conditions is 20 – 25% bigger than in the beam tests, that is demonstrated in Fig.12. This increase of noise is clearly due to the faster response of the ATLAS chain.

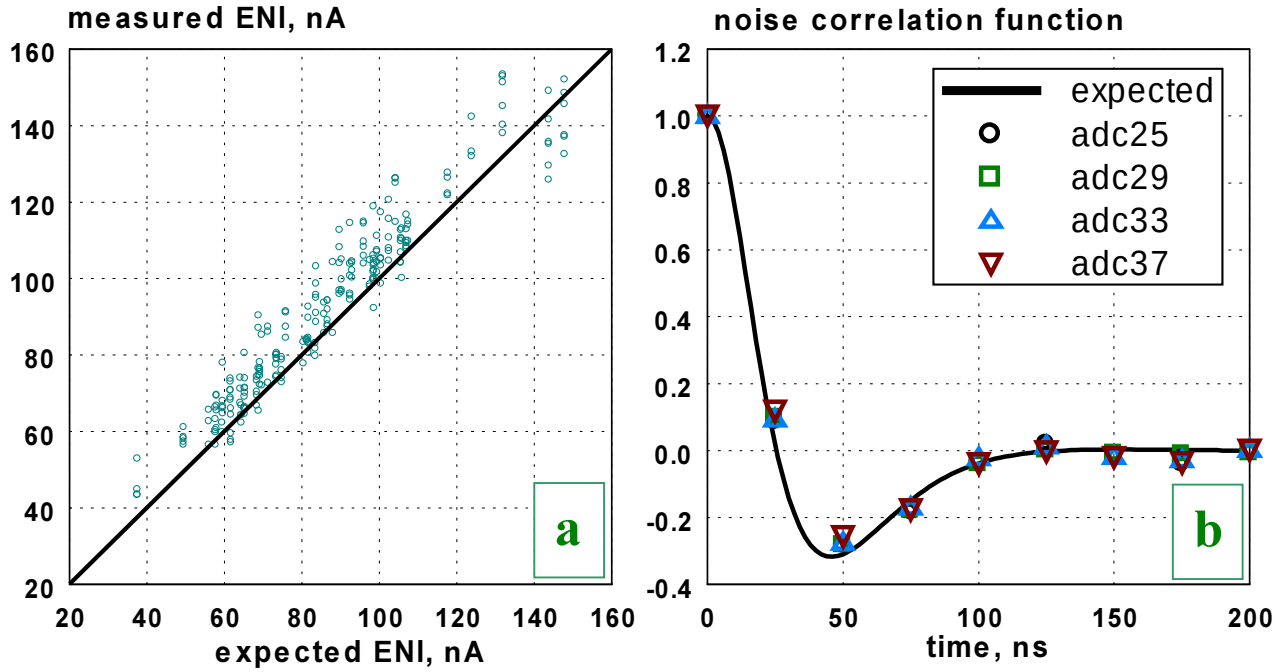

Figure 11: *Equivalent noise current (a) in test beam setup (points) vs. prediction by eq.33 (line) . Noise autocorrelation function (b) measured for 4 test beam channels (points) and calculation for readout channel 2 (line).*

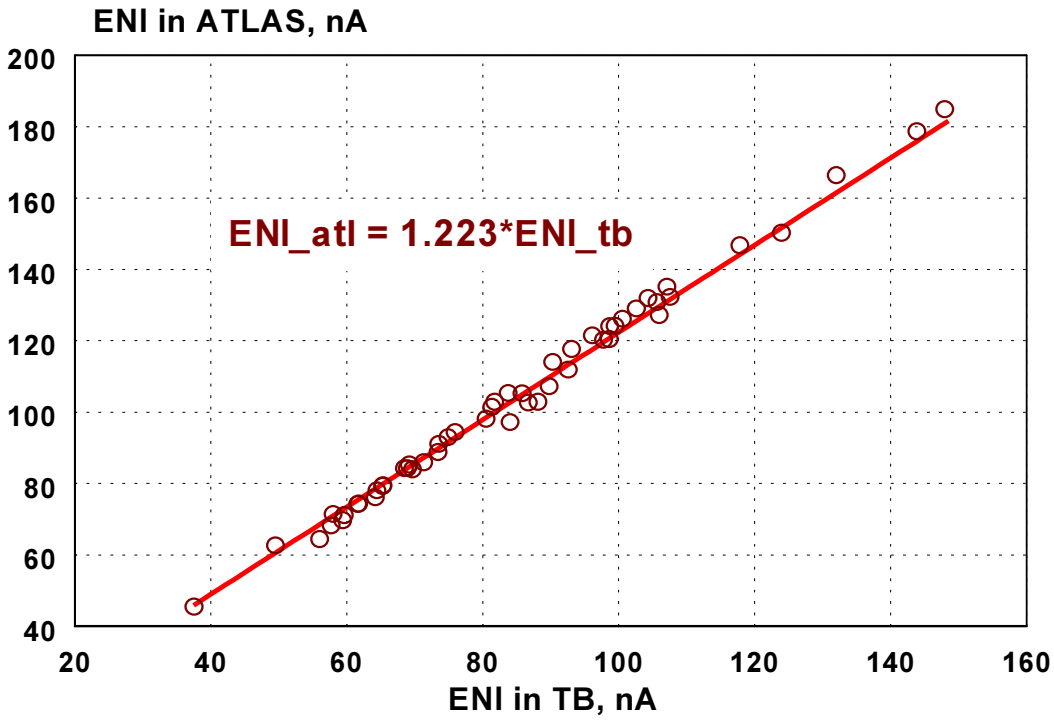

Figure 12: *Equivalent noise current calculated for the test beam nominal chain and for ATLAS conditions.*

8. CONCLUSIONS

The model function for the HEC calibration and signal chain is constructed in frequency domain. The signal waveform in time domain is calculated by applying the partial fractions expansion method. Typically the real calibration and ionization signals are described within precision of ±1% in full time window.

The set of parameters for the case of the test beam setup is obtained either on the basis of laboratory measurements or oscilloscope measurements in real conditions. Some parameters are not known yet for the final ATLAS setup since the final version of some components of the chain is not designed. So, the set of the ATLAS chain parameters presented here is preliminary and can be corrected in future. The nominal HEC ionization signal is calculated and the values of samples needed for the pileup simulations are produced.

The model for the electronic noise is created and compared to the test beam data. The expected ENI in ATLAS is ~20% bigger than in the test beam setup. The noise correlation coefficients are produced for all HEC readout channels for the further use in the readout driver studies.

References

[1] J.Colas, et al.
The LArg calorimeter calibration board.
ATLAS Internal Note, LARG-2000-006, Dec. 1999

[2] L.Kurchaninov,
HEC Cold Cables. Signal Shape Analysis
ATLAS HEC-Note-066, Dec. 1998

[3] W.D.Cwienk et al.
Preshaper for the Hadron Endcap Calorimeter. Design Review
ATLAS HEC-Note-094, Apr. 2000

[4] J.Colot, et al.
The LAr tri-gain shaper.
ATLAS Internal Note, LARG-No-92, Mar. 1998